Multi-scale Geometric Modeling of Ambiguous Shapes with Toleranced Balls and Compoundly Weighted α-shapes *

Frédéric Cazals and Tom Dreyfus

June 16, 2010

Contents

Abstract

Dealing with ambiguous data is a challenge in Science in general and geometry processing in particular. One route of choice to extract information from such data consists of replacing the ambiguous input by a continuum, typically a one-parameter family, so as to mine stable geometric and topological features within this family. This work follows this spirit and introduces a novel framework to handle 3D ambiguous geometric data which are naturally modeled by balls.

First, we introduce *toleranced balls* to model ambiguous geometric objects. A toleranced ball consists of two concentric balls, and interpolating between their radii provides a way to explore a range of possible geometries. We propose to model an ambiguous shape by a collection of toleranced balls, and show that the aforementioned radius interpolation is tantamount to the growth process associated with an additively-multiplicatively weighted Voronoi diagram (also called compoundly weighted or CW). Second and third, we investigate properties of the CW diagram and the associated CW α-complex, which provides a filtration called the λ-complex. Fourth, we sketch a naive algorithm to compute the CW VD. Finally, we use the λ-complex to assess the quality of models of large protein assemblies, as these models inherently feature ambiguities.

*Conference version: Symposium on Geometry Processing, 2010

1 Introduction

1.1 Voronoi Diagrams and Applications

The Voronoi diagram of a finite collection of sites equipped with a generalized distance is the cell decomposition of the ambient space into equivalence classes of points having the same nearest sites for this distance. Voronoi diagrams are central constructions in science and engineering [OC00], and their versatility actually comes from two sources. First, the great variability of sites and distances is a first source of diversity. While the most classical construction is the Euclidean distance diagram for points, the mere class of circles and weighted points yields as diverse diagrams as power, Apollonius and Möbius diagrams–see [BWY06] and Fig. 1. Second, the information encoded in a Voronoi diagram actually goes beyond the aforementioned cell decomposition. One can indeed consider the bisectors bounding the cells as the realization of a growth process defined by the distance, in the sense that the level sets of this distance intersect on the bisectors. This viewpoint motivated the development of α-complexes and α-shapes [Ede92], a beautiful construction providing a filtration of the Delaunay triangulation dual of the Voronoi diagram, later complemented by the flow complex [GJ03]. From a mathematical standpoint, these developments are concerned with the topological changes undergone by the sub-level sets of the distance, which is the heart of Morse theory [Mil63]. Ideas in this realm also motivated the development of topological persistence [ELZ02, CSEH05], a subject concerned with the assessment of the stability of topological features associated with the sub-level sets of a function defined on a topological space.

The success of α-shapes relies on two cornerstones. First, the aforementioned growth process gives access to a multi-scale analysis of the input sites. For example, the problem of reconstructing a shape from sample points can be tackled by considering the *space-filling diagram* consisting of balls grown around the sample points. Alas, a provably good reconstruction using this strategy requires a uniform sampling, which motivated the definition of more local growth processes. One may cite conformal α-shapes [CGPZ06], where the growth process depends on the distance of the samples to the medial axis, and the scale-axis transform [GMPW09] which provides a hierarchy of skeletal shapes based on a dilation (and retraction) of medial balls. Second, α-shapes inherently model objects represented by collections of balls—in particular molecules, and encode remarkable geometric and topological properties [Ede95]. For the particular case of proteins and small macro-molecular complexes, they have been instrumental to compute molecular surfaces [AE96] and model interfaces [BGNC09].

Our developments are precisely motivated by the requirement to perform multi-scale analysis in computational structural biology.

1.2 Contributions

Structural proteomics studies are concerned by the identification and the modeling of molecular machines operating within the cell [GAG$^+$06], and a major endeavour consists of modeling assemblies involving from tens [LTSW09] to hundreds [ADV$^+$07] of polypeptide chains. This modeling requires integrating data coming from several experimental sources, these data being typically noisy and incomplete [AFK$^+$08]. In this context, the premises just discussed on α-shapes certainly hold: on the one hand, balls are the primitive of choice since we deal with atoms and molecules; on the other hand, multi-scale analysis are in order since we deal with ambiguous data and need to accommodate uncertainties on the shapes and positions of proteins within an assembly. In this context, we make the following contributions.

First, we introduce toleranced balls to model ambiguous geometric shapes. A toleranced ball consists of two concentric balls—the *inner* and *outer* balls, and interpolating between them allows one to replace an arbitrary ball by one-parameter family of balls. As illustrated on Fig. 2, the inner (outer) ball of a toleranced ball is meant to accommodate high (low) confidence regions. We note in passing that our approach bears some similarities with modeling with toleranced parts in engineering, where tolerances are generally accommodated thanks to Minkowski sums [LWC97]. Second, we show that the growth process associated with this interpolation is associated with a so-called additively-multiplicatively-weighted Voronoi diagram, also called compoundly weighted Voronoi diagram—CW VD for short. Third, we investigate properties of this CW diagram and its dual. Fourth, we present the filtration, called the λ-complex, induced on the dual by the growth process, and encoding all possible topologies associated

with this growth process. Our analysis generalizes the so-called β-shapes [SCC+06], i.e. the α-shape associated to an Apollonius diagram [BD05, BWY06, EK06]. Fifth, we sketch an algorithm to compute the CW VD. Finally, we present experimental results on toleranced protein models. Due to the lack of space, proofs are omitted and the reader is referred [CD10].

2 Toleranced Models and Compoundly Weighted Voronoi Diagram

2.1 CW-distance and toleranced balls

Toleranced balls. Given a weighted point $S_i(c_i; \mu_i, \alpha_i)$, with center c_i and parameters (real numbers) $\mu_i > 0$ and α_i, we define the additively-multiplicatively distance as follows:

$$\lambda(S_i, p) = \mu_i \mid\mid c_i p \mid\mid -\alpha_i. \tag{1}$$

This distance is associated with so-called compoundly-weighted Voronoi diagrams or CW VD for short [OC00]. Geometrically speaking, this distance is best understood using the following growth process. Let a *toleranced ball* $\overline{S_i}(c_i; r_i^-, r_i^+)$ be a pair of concentric balls of radii $r_i^- < r_i^+$, centered at c_i. These balls are called the *inner* and *outer* balls. Given a toleranced ball $\overline{S_i}$ and a real parameter λ, consider the *grown ball* $\overline{S_i}[\lambda]$ centered at c_i and whose radius is defined by:

$$r_i(\lambda) = r_i^- + \lambda(r_i^+ - r_i^-). \tag{2}$$

Denoting $\delta_i = r_i^+ - r_i^-$, a point p is reached by this growth process once $r_i(\lambda) =\mid\mid c_i p \mid\mid$, that is

$$\lambda(\overline{S_i}, p) = \frac{\mid\mid c_i p \mid\mid}{\delta_i} - \frac{r_i^-}{\delta_i}. \tag{3}$$

In other words, a toleranced ball $\overline{S_i}(c_i; r_i^-, r_i^+)$ is tantamount to a weighted point $S_i(c_i; \mu_i = 1/\delta_i, \alpha_i = r_i^-/\delta_i)$; and reciprocally, a weighted point $S_i(c_i; \mu_i, \alpha_i)$ is tantamount to a toleranced ball $\overline{S_i}(c_i; r_i^- = \alpha_i/\mu_i, r_i^+ = (1+\alpha_i)/\mu_i)$. In the sequel, we shall use both terminologies and exchangeable refer to weighted point S_i or toleranced ball $\overline{S_i}$.

Toleranced tangency and generalization of the empty ball property. For affine (Apollonius) Voronoi diagrams, it is well known that for each point centered on a Voronoi face, there exists a unique ball orthogonal (tangent) to the balls associated with the vertices of the dual simplex, and conflict free with all the other balls. To derive the analogue in the CW-case, consider a point p and two toleranced balls $\overline{S_i}$ and $\overline{S_j}$ such that $\lambda(S_i, p) = \lambda < \lambda(S_j, p)$. For the pair $\overline{S_i}$ and p, one gets with Eq. (1):

$$\mid\mid p c_i \mid\mid -\frac{\alpha_i}{\mu_i} - \frac{\lambda}{\mu_i} = 0 \;\Leftrightarrow \mid\mid p c_i \mid\mid -r_i^- - \lambda\delta_i = 0. \tag{4}$$

Similarly, for the pair $\overline{S_j}$ and point p:

$$\mid\mid p c_j \mid\mid -\frac{\alpha_j}{\mu_j} - \frac{\lambda}{\mu_j} > 0 \;\Leftrightarrow \mid\mid p c_j \mid\mid -r_j^- - \lambda\delta_j > 0. \tag{5}$$

We summarize with the following definition, illustrated on Fig.3:

Definition. 1. *A ball $B(p, \lambda)$ which satisfies the condition of Eq. (4) w.r.t. a toleranced ball $\overline{S_i}$ is called* toleranced tangent *(TT for short) to $\overline{S_i}$. A toleranced ball $\overline{S_j}$ and a ball $B(p, \lambda)$ which satisfy the condition of Eq. (5) are called* conflict free*.*

Remark. 1. *Equation (4) states that the inner ball $B(c_i, r_i^-)$ and the ball $B(p, \lambda\delta_i)$—which is the ball $B(p, \lambda)$* scaled *by δ_i, are tangent. Similarly, condition (5) states that $B(c_j, r_j^-)$ and $B(p, \lambda\delta_j)$ do not intersect. We shall use this property to illustrate TT balls, see e.g. Fig. 3.*

Remark. 2. *Let $\overline{\mathcal{S}}$ be a collection of toleranced balls. Consider a ball $B(p,\lambda)$ which is TT to a subset of balls $T \subset \overline{\mathcal{S}}$, and conflict free with the toleranced balls in $\overline{\mathcal{S}}\backslash T$. The center p of this ball is found at the intersection of the spheres bounding the grown balls $\overline{S_i}[\lambda]$ with $\overline{S_i} \in T$, and is located outside the grown balls $\overline{S_j}[\lambda]$ with $\overline{S_j} \in \overline{\mathcal{S}}\backslash T$.*

3 The Compoundly Weighted Voronoi Diagram

Consider a collection $\overline{\mathcal{S}}$ of n toleranced balls. The Compoundly Weighted Voronoi diagram is the partition of the space according to the *nearest neighbor* relationship, for the CW distance, that is:

$$Vor(\overline{S_i}) = \{p \in \mathbb{R}^3 \mid \lambda(\overline{S_i}, p) \leq \lambda(\overline{S_j}, p) \forall j \neq i\}. \tag{6}$$

More generally, denoting T_{k+1} a tuple of $k+1$ toleranced balls, we are interested in $Vor(T_{k+1}) = \cap_{\overline{S_i} \in T_{k+1}} Vor(\overline{S_i})$. Naturally, we are also interested in the dual complex generalizing the Delaunay triangulation.

3.1 Bisectors in the CW case

The bisector of a tuple of toleranced balls T_{k+1} is the loci of points having the same CW distance w.r.t. every toleranced ball. We denote this bisector $\zeta(T_{k+1})$, and examine in turn the case for pairs, triples, and quadruples. Our analysis assumes that the δ_i are not equal, as this is the Apollonius case [BWY06].

3.1.1 Bisector of two toleranced balls

Analysis. Let $\overline{S_i}$ and $\overline{S_j}$ be two toleranced balls. The following property describes the existence of the bisector $\zeta(i,j)$ of $\overline{S_i}$ and $\overline{S_j}$:

Proposition. 1. *$\overline{S_i}$ is* trivial *w.r.t. toleranced ball $\overline{S_j}$ iff $\delta_i \leq \delta_j$ and the following condition, which states that c_i belongs to the interior of the Voronoi region of $\overline{S_j}$, holds:*

$$\lambda(\overline{S_j}, c_i) < -\frac{r_i^-}{\delta_i}. \tag{7}$$

Assuming that $\zeta(i,j)$ exists, its geometry depends on the relative values of δ_i and δ_j. Assuming w.l.o.g. that $\delta_i < \delta_j$, $\overline{S_j}$ grows faster than $\overline{S_i}$ so that for a large enough value of λ, the grown ball $\overline{S_i}[\lambda]$ is contained in its counterpart $\overline{S_j}[\lambda]$, so that the bisector is a closed surface, with c_i in the bounded region delimited by $\zeta(i,j)$. Matching the generalized distances shows that this surface is a degree-four algebraic surface. See Fig. 4 for a 2D illustration.

Extremal TT balls. If the bisector exists, it makes sense to track the TT balls such that the corresponding λ value is a local extremum. By radial symmetry w.r.t. the line joining the centers of the balls, such balls are necessarily centered at the intersection between the bisector and the line joining the centers. Assume w.l.o.g. that $\delta_i < \delta_j$. The minimal such ball, denoted $\underline{M}_{i,j}(\underline{m}_{i,j}, \underline{\rho}_{i,j})$ is such that $\overline{S_i}[\underline{\rho}_{i,j}]$ and $\overline{S_j}[\underline{\rho}_{i,j}]$ are tangent at $\underline{m}_{i,j}$. The maximal ball $\overline{M}_{i,j}(\overline{m}_{i,j}, \overline{\rho}_{i,j})$ is such that $\overline{S_i}[\overline{\rho}_{i,j}]$ is interior-tangent to $\overline{S_j}[\overline{\rho}_{i,j}]$ at $\overline{m}_{i,j}$.

The parameters of these extremal TT balls are computed as follows:

Proposition. 2. *The two extremal TT balls $B(p,\lambda)$ of two toleranced balls are characterized by*

$$\lambda = \frac{|| c_i c_j || - (\alpha r_i^- + \beta r_j^-)}{\alpha \delta_i + \beta \delta_j}, \tag{8}$$

and

$$\vec{c_i p} = \alpha \frac{\lambda \delta_i + r_i^-}{|| c_i c_j ||} \vec{c_i c_j}, \tag{9}$$

where $\alpha = \pm 1$ and $\beta = \pm 1$ depend on the ball processed (min or max) and the relative positions of $\overline{S_i}$ and $\overline{S_j}$ (case analysis in the proof).

3.1.2 Bisector of three toleranced balls

Analysis. Consider three toleranced balls $\overline{S_{i_0}}, \overline{S_{i_1}}, \overline{S_{i_2}}$ such that the bisector of each pair exists. To avoid the Apollonius case, we suppose without loss of generality that $\delta_{i_0} \leq \delta_{i_1} \leq \delta_{i_2}$ with $\delta_{i_0} < \delta_{i_2}$. If there is no intersection between $\zeta(i_0, i_1)$ and $\zeta(i_0, i_2)$, $\zeta(i_0, i_1, i_2)$ does not exist, and reciprocally. Assume that $\zeta(i_0, i_1, i_2)$ exists. Since at least one δ_i differs from the other two, there is at most one Apollonius bisector. The geometry of $\zeta(i_0, i_1, i_2)$ depends on $\delta_{i_0}, \delta_{i_1}$ and δ_{i_2}, and one faces the following cases.

▷ **CWB.III.1** If there is no Apollonius bisector, $\zeta(i_0, i_1, i_2)$ is a bounded curve resulting from the intersection of two CW bisectors.
▷ **CWB.III.2** If the Apollonius bisector is not a half straight line, $\zeta(i_0, i_1, i_2)$ is a bounded curve resulting from the intersection of one CW bisector, and one sheet of a hyperboloid (possibly degenerated to a hyperplane).
▷ **CWB.III.3** If the Apollonius bisector is a half straight line, $\zeta(i_0, i_1, i_2)$ is reduced to at most two intersection points. Note that if there are two intersection points, $\delta_{i_1} = \delta_{i_2}$ and $\overline{S_{i_1}}$ is included in and tangent to $\overline{S_{i_2}}$.

Extremal TT balls. In any case, there are two (possibly identical) extremal TT balls. If one bisector is a half straight line, these balls are found by intersecting this line with one of the other two bisectors. In the general case, identifying these two balls involves four equations in four unknowns—the coordinates of the center and the weight λ. Denote π the plane defined by the centers of the three balls. The growth of the balls being symmetric with respect to this plane, the fourth equation consists of constraining the center of an extremal TT ball to plane π. The calculation is covered by the following proposition for $k = 2$:

Proposition. 3. *Let $T_{k+1} = \{\overline{S_{i_j}}\}_{j=0,\ldots,k}$ be a triple or quadruple of toleranced balls, i.e. $k = 2$ or $k = 3$. Computing the two extremal TT balls of the tuple T_{k+1} requires solving a degree four equation. A value solution λ of this equation is valid provided that $\lambda\delta_{i_j} + r_{i_j}^- \geq 0$, $\forall j = 0, \ldots, k$.*

Geometrically, three intersecting spheres generically intersect in two points. The extreme TT balls correspond to the situations where these two points coalesce.

3.1.3 Bisector of four toleranced balls

Analysis. Consider four toleranced balls $\overline{S_{i_0}}, \overline{S_{i_1}}, \overline{S_{i_2}}, \overline{S_{i_3}}$ such that the bisector of each pair exists. To avoid the Apollonius case, we suppose w.l.o.g. that $\delta_{i_0} \leq \delta_{i_1} \leq \delta_{i_2} \leq \delta_{i_3}$ with $\delta_{i_0} < \delta_{i_3}$. If the intersection of $\zeta(i_0, i_1)$, $\zeta(i_0, i_2)$ and $\zeta(i_0, i_3)$ is empty, the intersection of all bisectors of pairs is empty and $\zeta(i_0, i_1, i_2, i_3)$ does not exist, and reciprocally. If $\zeta(i_0, i_1, i_2, i_3)$ exists, we have $\zeta(i_0, i_1, i_2, i_3) = \zeta(i_0, i_3) \cap \zeta(i_1, i_2, i_3)$, from which the following analysis follows.

▷ **CWB.IV.1** The bisectors $\zeta(i_0, i_3)$ and $\zeta(i_1, i_2, i_3)$ being a surface and a curve, their generic intersection, if any, consists of a finite set of points. As we shall see below, there are at most four such points.
▷ **CWB.IV.2** As a degenerate case, when $\zeta(i_1, i_2, i_3)$ is a bounded curve, the intersection of $\zeta(i_1, i_2, i_3)$ and $\zeta(i_0, i_3)$ may be $\zeta(i_1, i_2, i_3)$. In this case, $\zeta(i_0, i_1, i_2, i_3)$ has the geometry of the bisector $\zeta(i_1, i_2, i_3)$ of three toleranced balls.

Extremal balls. We distinguish two cases. If $\zeta(i_0, i_1, i_2, i_3)$ has the geometry of a bisector of three toleranced balls, we refer to the analysis carried out in section 3.1.2. Otherwise, $\zeta(i_0, i_1, i_2, i_3)$ is reduced to at most four points, as shown by the following constructive proof of proposition 3:

3.2 Voronoi Diagram and its Dual Complex

Empty Voronoi regions. A toleranced ball whose region is empty is called trivial. Proposition 1 gives a condition of triviality for two toleranced balls. But triviality of a toleranced ball amidst a collection of balls is more complex, since a toleranced ball might not be trivial w.r.t. any other one, yet, it might be trivial with respect to their union. It can be checked that a toleranced ball $\overline{S_i}$ is trivial w.r.t. a tuple of balls T provided that $\overline{S_i}[\lambda] \subset \bigcup_{\overline{S_j} \in T} \overline{S_j}\lambda$ for all values of λ.

Dual Complex. The Voronoi region $Vor(T_{k+1})$ of a tuple T_{k+1} may have several connected components, each being termed a *face*. Each such face corresponds to the intersection of $k+1$ Voronoi regions, so that we associate an *abstract simplex* or *simplex* for short in the dual complex. That is, if $Vor(T_{k+1})$ consists of m faces, on finds $\Delta_j(T_{k+1}), j \in 1, \ldots, m$ simplices in the dual complex. (The multiplicity is omitted if the tuple T_{k+1} yields a single simplex.) Assuming that the input toleranced balls are numbered from 1 to n, a simplex is *identified* by a list of integers, and inclusion between such lists defines a partial order on simplices. We therefore represent the dual complex by a Hasse diagram D_S with one node per simplex. Note that we may also (arbitrarily) embed a simplex within the union of Voronoi faces it is associated with. See Fig. 5.

Topological complications. A Voronoi region gets sandwiched between two neighbors when the corresponding toleranced ball defines a *lens* between the Voronoi region of two neighboring toleranced balls, a case also found in the Apollonius diagram. In the dual complex, the vertex of this toleranced balls has exactly two neighbors and the triangle corresponding to these three toleranced balls does not have any coface.

A Voronoi region might not be connected, and this may happen for tuples of size one to four. We illustrate this in 2D with Fig. 5. For a toleranced ball, consider $\overline{S_4}$ whose Voronoi region is split into two faces, associated with the vertices (zero-dimensional simplices) $\Delta_1(4)$ and $\Delta_2(4)$ in the Hasse diagram. For two toleranced balls, note that the Voronoi region $Vor(\overline{S_1}, \overline{S_2})$ consists of two faces—open line segments in this case, yielding the simplices $\Delta_1(1,2)$ and $\Delta_2(1,2)$ in the Hasse diagram. For three toleranced balls, note that the triple $(\overline{S_1}, \overline{S_2}, \overline{S_4})$ corresponds to two triangles.

A Voronoi region may not be simply connected. When one toleranced ball punches a hole into a face, the corresponding one-simplex does not have any coface. See e.g. toleranced ball $\overline{S_7}$ and the simplex $\Delta(2,7)$ on Fig. 5. When two toleranced balls punch a hole into a Voronoi region, the two-simplex they define does not have any coface either. Finally when three toleranced balls punch a hole into a Voronoi region, two tetrahedra of the dual complex share the same vertices, the same edges and same triangles. This latter case is illustrated in 2D, where a hole punched by two toleranced balls in a Voronoi region results in two triangles with the same vertices and the same edges. See $\Delta_1(2,5,6)$ and $\Delta_2(2,5,6)$ on Fig. 5.

Bounded and Unbounded Voronoi regions. A toleranced ball $\overline{S_i} \in \overline{\mathcal{S}}$ is called *maximal* w.r.t. to $\overline{\mathcal{S}}$ if $\delta_i \geq \delta_j, \forall j \neq i$. A toleranced ball which is not maximal has a bounded Voronoi region in the CW VD of $\overline{\mathcal{S}}$, and the subset of maximal toleranced balls is denoted $\overline{\mathcal{S}}_{\max}$. The CW VD diagram of toleranced balls in $\overline{\mathcal{S}}_{\max}$ is an Apollonius diagram since all δ_i are equal, and a subset of balls in $\overline{\mathcal{S}}_{\max}$ have an unbounded Voronoi region. Mimicking the affine case, a simplex is said to lie on the convex hull $CH(\overline{\mathcal{S}})$ of the dual complex if its dual Voronoi face is unbounded. The vertices of such simplices belong to $\overline{\mathcal{S}}_{\max}$.

4 Space-filling diagram and λ-complex

In this section, we investigate the domain $\mathcal{F}_\lambda = \cup \overline{S_i}[\lambda]$ defined by the union of growing balls. We present the λ-complex filtration of the dual complex. The reader is referred to [Ede92] for the affine weighted α-complex.

4.1 Gabriel and dominated simplices

In the affine case, changes in the α-complex are associated with Gabriel simplices: a Gabriel simplex $\Delta(T)$ is a simplex such that its minimal orthogonal ball $\underline{M}_T$ is conflict free, and the simplex enters the α-complex when $\lambda \geq \underline{\rho}_T$, with $\underline{\rho}_T$ the weight of $\underline{M}_T$. The generalization to the CW setting is not straightforward since Voronoi regions might not be connected, and also since a tuple T generally has two extremal TT balls, respectively denoted $\underline{M}_T(\underline{m}_T, \underline{\rho}_T)$ and $\overline{M}_T(\overline{m}_T, \overline{\rho}_T)$. We now examine these two balls and refer the reader to Fig. 6 for an illustration. (To examine this figure, recall that a TT ball $M(p,\lambda)$ is conflict free with a toleranced ball $\overline{S_i}$ iff the scaled version of M by δ_i i.e. $M(p, \delta_i\lambda)$ does not intersect the inner ball of $\overline{S_i}$.)

Minimal TT balls and Gabriel simplices. If the center $\underline{m}_T$ of the minimal TT ball $\underline{M}_T$ belongs to the relative interior of a Voronoi face of the tuple, or equivalently the ball is conflict free, the simplex is called *Gabriel*.

Maximal TT balls and domination of simplices. For a simplex $\Delta(T)$, consider the intersection of the spheres bounding the grown balls, i.e.

$$I_T[\lambda] = \cap_{\overline{S_i} \in T} \partial \overline{S_i}[\lambda]. \tag{10}$$

In 3D, if T is a $k+1$ tuple, $I_T[\lambda]$ is generically a $2-k$-sphere. Consider now a tuple such that the δ_i of its balls are not all equal, and assume that $T = A \cup B$, with A the balls realizing the maximum δ_i in the tuple. The corresponding bisector is bounded and has a unique maximal TT ball $\overline{M}_T$. If this ball is conflict free, the spheres bounding the grown balls in T intersect until $I_T[\lambda]$ reduces to the point $\overline{m}_T$. Beyond that point, the intersection of the spheres bounding grown balls in B is contained in the union of the grown balls in A. That is, as opposed to the Euclidean setting, the simplex $\Delta(T)$ does not catch a coface. The simplex $\Delta(T)$ whose Voronoi face contains $\overline{m}_T$ is called *dominant*.

Similarly, consider a simplex $\Delta(U)$ which is an ancestor of the dominant simplex $\Delta(T)$ in the Hasse diagram, with $B \subset U \subsetneq T$. (An ancestor is any node found on a path joining a zero simplex to $\Delta(T)$.) Such a simplex does not catch any coface either when point $\overline{m}_T$ is reached by the growing balls. All such simplices are called *dominated*. To identify the moment in time where simplex $\Delta(U)$ gets dominated, we introduce

$$\gamma_{\Delta(U)} = \overline{\rho}_{\Delta(T)}. \tag{11}$$

The condition $B \subset U \subsetneq T$ actually yields 2 cases, namely (i) $U = B$, or (ii) $B \subsetneq U \subsetneq T$. In three dimensions, enumerating these possibilities yields the following cases:

▷ **Dom.1** $T = \{\overline{S_1}, \overline{S_2}\}$ with $\delta_1 > \delta_2$: case (i) that is $U = \{\overline{S_2}\}$.

▷ **Dom.2** $T = \{\overline{S_1}, \overline{S_2}, \overline{S_3}\}$ with $\delta_1 > \delta_2 \geq \delta_3$: case (i) that is $U = \{\overline{S_2}, \overline{S_3}\}$.

▷ **Dom.3** $T = \{\overline{S_1}, \overline{S_2}, \overline{S_3}\}$ with $\delta_1 = \delta_2 > \delta_3$: case (i) that is $U = \{\overline{S_3}\}$, and case (ii) that is $U = \{\overline{S_1}, \overline{S_3}\}$ or $U = \{\overline{S_2}, \overline{S_3}\}$.

By convention and since a 4-tuple yields a discrete set of at most four tetrahedra, we say that a 3-simplex cannot be dominant—which prevents a 2-simplex from being dominated. Also, a 0-simplex cannot be dominant. Dominant and dominated simplices are important to describe the evolution of the boundary $\partial\mathcal{F}_\lambda$: upon getting dominated, a simplex does not contribute to $\partial\mathcal{F}_\lambda$ anymore.

4.2 The λ-complex Filtration

The filtration. Equipped with Gabriel simplices, the following mimics the Euclidean setting:

Definition. 2. *The λ-complex K_λ is a subset of the dual complex defined as follows: a simplex $\Delta(T)$ belongs to K_λ iff (i) $\Delta(T)$ is Gabriel and $\lambda \geq \underline{\rho}_{\Delta(T)}$, or (ii) $\Delta(T)$ is a face of $\Delta(U)$ with $\Delta(U) \in K_\lambda$.*

Increasing λ results in a nested sequence of (abstract) simplicial complexes, which eventually coincide with the dual complex, so that the collection of λ-complexes forms a filtration.

Status of simplices. The status of a simplex in the affine setting is described from the topology of its link. In the CW case, the presence of simplices without any coface as described in section 3.2 requires devising different classification criteria. For a simplex $\Delta(T)$, consider the intersection $I_T[\lambda]$ of Eq. (10). Upon increasing λ, this intersection sweeps the Voronoi region of the tuple. We base our classification on the portion of the Voronoi region swept by $I_T[\lambda]$ up to time λ. That is, a k-simplex of K_λ is classified as follows:

– *Singular*: the region swept by $I_T[\lambda]$ up to time λ is contained in the relative interior of the dual of the simplex.
– *Interior*: the region swept by $I_T[\lambda]$ up to time λ contains the dual of the simplex in its interior.
– *Regular*: neither singular nor interior.

Table 1 Classification of simplices : cases.

Case
(1) $\Delta(T) \in CH(\overline{\mathcal{S}})$,Gabriel, non dominated/dominant
(2) $\Delta(T) \in CH(\overline{\mathcal{S}})$,non Gabriel, non dominated/dominant
(3) $\Delta(T) \notin CH(\overline{\mathcal{S}})$ Gabriel, non dominated/dominant
(4) $\Delta(T) \notin CH(\overline{\mathcal{S}})$,non Gabriel, non dominated/dominant
(5) $\Delta(T) \notin CH(\overline{\mathcal{S}})$ Gabriel, dominant
(6) $\Delta(T) \notin CH(\overline{\mathcal{S}})$,non Gabriel, dominant
(7) $\Delta(T) \notin CH(\overline{\mathcal{S}})$ Gabriel, dominated
(8) $\Delta(T) \notin CH(\overline{\mathcal{S}})$,non Gabriel, dominated

Table 2 Classification of simplices : intervals.

(1) $(\underline{\rho}_{\Delta(T)}, \underline{\mu}_{\Delta(T)}]$	$(\underline{\mu}_{\Delta(T)}, +\infty]$	
(2)	$(\underline{\mu}_{\Delta(T)}, +\infty]$	
(3) $(\underline{\rho}_{\Delta(T)}, \underline{\mu}_{\Delta(T)}]$	$(\underline{\mu}_{\Delta(T)}, \overline{\mu}_{\Delta(T)}]$	$(\overline{\mu}_{\Delta(T)}, +\infty]$
(4)	$(\underline{\mu}_{\Delta(T)}, \overline{\mu}_{\Delta(T)}]$	$(\overline{\mu}_{\Delta(T)}, +\infty]$
(5) $(\underline{\rho}_{\Delta(T)}, \underline{\mu}_{\Delta(T)}]$	$(\underline{\mu}_{\Delta(T)}, \overline{\rho}_{\Delta(T)}]$	$(\overline{\rho}_{\Delta(T)}, +\infty]$
(6)	$(\underline{\mu}_{\Delta(T)}, \overline{\rho}_{\Delta(T)}]$	$(\overline{\rho}_{\Delta(T)}, +\infty]$
(7) $(\underline{\rho}_{\Delta(T)}, \underline{\mu}_{\Delta(T)}]$	$(\underline{\mu}_{\Delta(T)}, \gamma_{\Delta(T)}]$	$(\gamma_{\Delta(T)}, +\infty]$
(8)	$(\underline{\mu}_{\Delta(T)}, \gamma_{\Delta(T)}]$	$(\gamma_{\Delta(T)}, +\infty]$

4.3 CW Classification of simplices

To classify simplices, we adopt the notations used in the affine case [Ede92] and denote $\underline{\mu}_{\Delta(T)}$ and $\overline{\mu}_{\Delta(T)}$ the λ-values such that a simplex becomes regular and interior.

For the affine α-complex, the classification of a simplex as singular, regular, or interior requires considering the four cases { Gabriel, not Gabriel } $\times$ { on the convex hull, not on the convex hull }. For simplices which are neither dominant nor dominated, these four possibilities are also found in the CW case—lines 1-4 of Table 2.

On the other hand, dominant and dominated simplices are not found on the convex hull—each such simplex involves at least one non-maximal ball, and always end up interior since the maximal TT ball of the tuple of a dominant simplex is conflict free. For dominant simplices, the two additional cases to be considered are Gabriel and non Gabriel—lines 5-6 in Table 2. Such a simplex becomes interior as soon as $\lambda \geq \overline{\rho}_{\Delta(T)}$.
Similarly for dominated simplices, the two additional cases to be considered are Gabriel and non Gabriel—lines 7-8 in Table 2. Recall that a dominated simplex is always associated to a dominant simplex. Using the weight $\gamma_{\Delta(T)}$ of the maximal TT ball of the tuple of the dominant simplex associated to the dominated simplex, see Eq. (11), the dominated simplex becomes interior as soon as $\lambda \geq \gamma_{\Delta(T)}$.

These notions are illustrated on Fig. 7, which features the restricted Voronoi diagram, i.e. the grown balls restricted to their Voronoi regions. Note in particular that the status of simplices reads from the relative position of the restriction w.r.t. the associated Voronoi face, as specified in section 4.2.

5 Implementation and Experiments

5.1 Algorithm

We designed and implemented an output sensitive algorithm computing the dual complex, with cubic pre-processing time. The algorithm also accommodates the *reduced λ-complex* i.e. the λ-complex restricted to values $\lambda \leq \lambda_{\max}$—that is the growth process if performed up to $\lambda_{\max}$.

The pre-processing consists of finding all tuples possibly contributing to the λ-complex for $\lambda \leq \lambda_{\max}$. Up to triples, a tuple is candidate provided that its minimal TT ball has a radius less than $\lambda_{\max}$. A

quadruple is candidate if at least one radius of its TT balls is less than $\lambda_{\max}$.

Based on these candidate tuples, the algorithm consists of two steps. First, one 3-simplex is created for each solution of the quartic equation mentioned in proposition 3, provided that this solution defines a conflict free TT ball. Second, the k-skeleton of the CW VD is incrementally built, from $k = 1$ to $k = 3$. To build the k-skeleton, the cofaces of every possible simplex are retrieved from the $(k-1)$-skeleton, and these cofaces are used to build the boundary of the Voronoi faces contributed by the tuple. The reader is referred to [CD10] for a precise description. We briefly comment on the implementation sketch which is interesting due to the interplay between the combinatorial, geometric, and algebraic levels.

5.2 Implementation

Sketch. The implementation follows the CGAL spirit, see `http://www.cgal.org`, and we sketch it in terms of *concepts* (a set of requirements) and *models* (a particular implementation). The class `CW_dual` representing the dual complex is templated by a combinatorial class providing the Hasse diagram representation, and by a geometric concept class `CWGeometricKernel` providing the predicates and constructions required. The corresponding generic model `CW_geometric_kernel` is itself templated by a concept class `AlgebraicKernel` providing the operations needed to deal with the extremal TT balls. As specified by propositions 2 and 3, computing these TT balls requires solving linear systems or a degree four algebraic equation, while the conflict free test requires evaluating the conflict_free predicate of Eq. (5). We implemented a model of the `AlgebraicKernel` named `CW_algebraic_kernel_double` which uses CGAL's `Algebraic_kernel_d_1`—the latter provides efficient operations on univariate polynomials. The number type being *double*, this kernel does not provide exact predicates. Finally, the class `CW_alpha_shape` inherits from `CW_dual` and provides the tags and intervals detailed in Table 2.

5.3 Application to molecular models

Reconstructing Large Assemblies. Understanding the behaviour of living cells requires describing the structure and behaviour of a number of macro-molecular assemblies. While atomic models of small complexes can be obtained from X ray crystallography and/or NMR, the reconstruction of large assemblies such as molecular motors (cell locomotion), branched actin filaments (muscle contraction), chaperonin cavities (protein folding) or nuclear pore complexes (nucleo-cytoplasmic regulation) is more challenging. A recent trend in this context consists of performing the reconstruction from diverse experimental data [AFK$^+$08]. For example, cryo electron microscopy (EM) maps allows the reconstruction of envelopes of assemblies, typically at intermediate resolution (10-15 Å). Immuno-labelling combined with EM can be used to locate protein instances, but positioning uncertainties are faced due to the resolution of microscopes. Proteomics methods such as Tandem Affinity Purification provide lists of interacting proteins, but these are inherently ambiguous. The reconstruction of a model from such noisy and ambiguous data is clearly a challenge, and typical reconstruction procedures perform simulating annealing in the space of parameters describing the model, so as to maximize the agreement between this model and the experimental data available. We now examine the largest protein assembly known to date in eukaryotic cells, namely the Nuclear Pore Complex (NPC).

Application to The Nuclear Pore Complex. The NPC is a radially symmetric protein assembly regulating exchanges between the nucleus and the cytoplasm of eukaryotic cells, thanks to the lumen located in its center. The NPC involves 456 protein *instances* of 30 different protein *types*, and we term each connected subset of instances a *complex* in the sequel. The *stoichiometry* of a protein type is the number of its instances—a number in the range 8-16 for the NPC. Two remarkable papers reported putative models of the NPC, reconstructed from the integration of various experimental data [ADV$^+$07, AFK$^+$08]. A model of the NPC is a collection of balls. The reconstruction resorts to simulated annealing to define the balls (centers and radii) so as to maximize the agreement with experimental data. The whole procedure is very complex—the supplemental of the two Nature papers runs on 107 pages, and different levels of detail are actually used along the optimization procedure. At the finest level, which corresponds to the output, a given protein is represented by a number of balls in the range 1–12, depending on the protein type. The functional optimized being non convex, a total of 1000 models were selected. These

models were further averaged to produce one density map per protein type, i.e. a 3D matrix where each pixel is endowed with the probability of being covered by an instance of that type. Refer to Fig. 2 for a 2D example. The maps being quite noisy, contouring a map does not in general allow one to precisely locate the instances of that type. Also, superimposing the 30 maps do not allow one to investigate the relative positions of the instances of all types. We use λ-shapes to make a collective assessment of these maps.

Applications of λ-shapes. As a pre-processing, we build a toleranced model for each map, based on its stoichiometry. The high confidence regions are defined as (clusters of) local maxima of the density. Starting from these anchors, a region growing algorithm is run until a region with prescribed volume is reached. Each connected component is then covered with one toleranced ball. Merging the toleranced models of the 30 types yields a toleranced model of the NPC consisting of 456 toleranced balls. The resulting reduced λ-complex for $\lambda_{\max} = 1$, computed in 11 minutes on an x86_64 bits architecture at 3.2HGz, is used for two purposes.

First, the topological persistence of connected components provides an assessment of the stability of complexes in the assembly. Our particular interest are the *stable* complexes, whose composition in terms of protein types can be discussed w.r.t. the aforementioned Tandem Affinity Purification data. Such a discussion will be reported elsewhere.

Second, we investigate the packing properties of instances : upon increasing λ, the number of connected components (#c.c.) of $\mathcal{F}_\lambda$ decreases, and its volume Vol_λ increases. The volume of a protein instance being estimated from its sequence of amino-acids, let Vol_{ref} the sum of the volumes of all instances, and denote $r_\lambda = Vol_\lambda / Vol_{ref}$. Tracking the evolution of the number #c.c. thanks to a Union-Find algorithm applied to the simplices of the dual complex, we investigate the correlations between the three parameters $(\#c.c., \lambda, r_\lambda)$.
This curve is presented on Fig. 8 for the 32 protein instances of a half-spoke, i.e. one of the 16 sub-units of the NPC. For a perfectly accurate model, one would expect one connected component for a value of $r_\lambda = 1$, but we observe 10 of them in our case. Also, the last two consecutive values of λ triggering a drop of the number of c.c. are as follows: for $\lambda = 0.62$, there are two c.c. and $r_{0.62} = 3.46$; for $\lambda = 1.25$, there is one c.c. and $r_{1.25} = 7.20$. The corresponding grown balls are illustrated on Fig. 9. On this example, the fact that a 7-fold increase of volume occupancy is required to connect the instances hints at an imprecise positioning of selected proteins. In particular, the significant increase of r_λ in-between $\#c.c. = 2$ and $\#c.c. = 1$ hints at a poor positioning of two instances located far away from the 30 remaining ones.

This type of analysis is being used to provide a thorough evaluation of putative pseudo-atomic NPC models, based on (i) the stability of complexes measured by topological persistence, (ii) a coherence analysis of the models w.r.t. Tandem Affinity Purification data, and (iii) quantitative statistics based on volume and surface calculations. These analysis will complement the qualitative discussions and hypothesis developed in [ADV+07].

6 Conclusion and outlook

Handling ambiguous geometric shapes is non trivial, and the spirit of this work is to integrate modeling uncertainties in the geometric model, as opposed to making arbitrary decisions. As demonstrated, the problem of modeling with toleranced balls is tantamount to using a compoundly weighted Voronoi diagram, and the fact that a toleranced ball (or equivalently a weighted point) has two parameters provides additional modeling flexibility. Yet, a number of further developments are called for.

On the algorithmic side, designing an efficient algorithm to build the dual complex of the CW VD is an open question. While our algorithm fits our needs in molecular modeling, an efficient algorithm is a must for the framework to be used say in geometry processing. From a combinatorial perspective, the task is difficult though, in particular because Voronoi regions are not connected. From a numerical perspective, designing efficient predicates based on degree-four algebraic numbers is also challenging. Finally, the design of toleranced models also raises interesting questions falling in the realm of geometric optimization.

On the application side, toleranced models should have a clear leveraging power in computational structural biology. A major trend there is the reconstruction of large molecular machines from the integration of various experimental data. The models designed so far are not precise enough to be used for mechanistical simulations. We believe that toleranced models have the potential to allow for a precise assessment of such models with respect to biological data, and will help to establish atomic-resolution models.

More classical geometric applications should also benefit from toleranced models, in particular the representation of shapes based on skeletal representations and the medial axis transform, in the spirit of recent contributions such as conformal α-shapes and scale-axis transforms.

Acknowledgements. Svetlana Dokudovskaya is acknowledged for stimulating discussions. Michael Hemmer is acknowledged for his help with CGAL's algebraic kernel.

References

[ADV+07] F. Alber, S. Dokudovskaya, L.M. Veenhoff, W. Zhang, J. Kipper, D. Devos, A. Suprapto, O. Karni-Schmidt, R. Williams, B.T. Chait, et al. The molecular architecture of the nuclear pore complex. *Nature*, 450(7170):695–701, 2007.

[AE96] N. Akkiraju and H. Edelsbrunner. Triangulating the surface of a molecule. *Discrete Appl. Math.*, 71:5–22, 1996.

[AFK+08] F. Alber, F. Forster, D. Korkin, M. Topf, and A. Sali. Integrating diverse data for structure determination of macromolecular assemblies. *Ann. Rev. Biochem.*, 77:11.1–11.35, 2008.

[BD05] J.-D. Boissonnat and C. Delage. Convex hull and voronoi diagram of additively weighted points. In *ESA*, 2005.

[BGNC09] B. Bouvier, R. Grunberg, M. Nilges, and F. Cazals. Shelling the voronoi interface of protein-protein complexes reveals patterns of residue conservation, dynamics and composition. *Proteins: structure, function, and bioinformatics*, 76(3):677–692, 2009.

[BWY06] J-D. Boissonnat, C. Wormser, and M. Yvinec. Curved voronoi diagrams. In J.-D. Boissonnat and M. Teillaud, editors, *Effective Computational Geometry for curves and surfaces*. Springer-Verlag, Mathematics and Visualization, 2006.

[CD10] F. Cazals and T. Dreyfus. Multi-scale geometric modeling of ambiguous shapes with toleranced balls and compoundly weighted α-shapes. Research Report RR-7306, INRIA, 2010.

[CGPZ06] F. Cazals, J. Giesen, M. Pauly, and A. Zomorodian. The conformal alpha shapes filtration. *The Visual Computer*, 22:1–10, 2006.

[CSEH05] D. Cohen-Steiner, H. Edelsbrunner, and J. Harer. Stability of persistence diagrams. In *ACM Symp. Comp. Geometry*, 2005.

[Ede92] H. Edelsbrunner. Weighted alpha shapes. Technical Report UIUCDCS-R-92-1760, Dept. Comput. Sci., Univ. Illinois, Urbana, IL, 1992.

[Ede95] H. Edelsbrunner. The union of balls and its dual shape. *Discrete Comput. Geom.*, 13:415–440, 1995.

[EK06] I.Z. Emiris and M.I. Karavelas. The predicates of the Apollonius diagram: algorithmic analysis and implementation. *Computational Geometry: Theory and Applications*, 33(1-2):18–57, 2006.

[ELZ02] H. Edelsbrunner, D. Letscher, and A. Zomorodian. Topological persistence and simplification. *Discrete Comput. Geom.*, 28:511–533, 2002.

[GAG+06] Anne-Claude Gavin, Patrick Aloy, Paola Grandi, Roland Krause, Markus Boesche, Martina Marzioch, Christina Rau, Lars Juhl Jensen, Sonja Bastuck, Birgit Dmpelfeld, Angela Edelmann, Marie-Anne Heurtier, Verena Hoffman, Christian Hoefert, Karin Klein, Manuela Hudak, Anne-Marie Michon, Malgorzata Schelder, Markus Schirle, Marita Remor, Tatjana Rudi, Sean Hooper, Andreas Bauer, Tewis Bouwmeester, Georg Casari, Gerard Drewes, Gitte Neubauer, Jens M Rick, Bernhard Kuster, Peer Bork, Robert B Russell, and Giulio Superti-Furga. Proteome survey reveals modularity of the yeast cell machinery. *Nature*, 440(7084):631–636, Mar 2006.

[GJ03] J. Giesen and M. John. The flow complex: A data structure for geometric modeling. In *ACM SODA*, 2003.

[GMPW09] J. Giesen, B. Mikls, M. Pauly, and C. Wormser. The scale axis transform. In *ACM Symp. on Computational Geometry*, 2009.

[LTSW09] K. Lasker, M. Topf, A. Sali, and H.J. Wolfson. Inferential Optimization for Simultaneous Fitting of Multiple Components into a CryoEM Map of Their Assembly. *Journal of Molecular Biology*, 388:180–194, 2009.

[LWC97] J-C. Latombe, R. Wilson, and F. Cazals. Assembly sequencing with toleranced parts. *Computer Aided Design*, 29(2):159–174, 1997.

[Mil63] John W. Milnor. *Morse Theory*. Princeton University Press, Princeton, NJ, 1963.

[OC00] A. Okabe and B. Boots K. Sugihara S. Nok Chiu. *Spatial Tessellations: Concepts and Applications of Voronoi Diagrams (2nd Ed.)*. Wiley, 2000.

[SCC+06] J. Seo, Y. Cho, C-H. Cho, D. Kim, J. Ryu, and D-S. Kim. The β-shape and β-complex for three-dimensional spheres. *Proceedings of the third International Symposium on Voronoi Diagrams in Science and Engineering*, 2006.

Figure 1 Curved Voronoi diagrams of 7 circles / weighted points. (a) Power diagram $d(S_i(c_i, r_i), p) = \|p - c_i\|^2 - r_i^2$. (b) Apollonius diagram : $d(S_i(c_i, r_i), p) = \|p - c_i\| - r_i$ (c) Möbius diagram : $d(S_i(c_i, a_i, r_i), p) = a_i\|p - c_i\|^2 - r_i^2$.

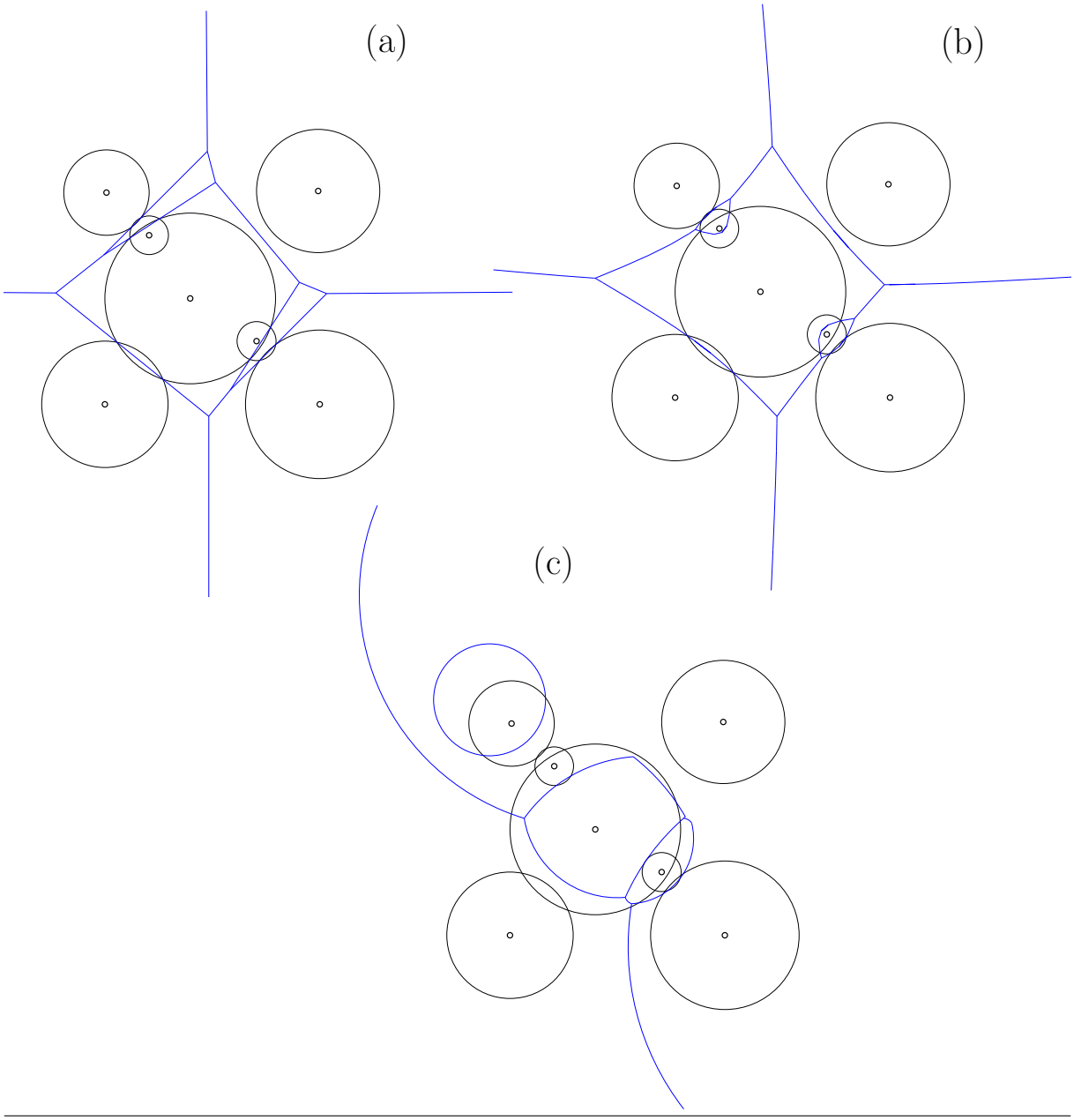

Figure 2 A fictitious molecule of three atoms undergoing conformational changes.(Inset) The two extreme conformations. (Main figure) Probability density map D and toleranced balls. The map D displays the probability for a given pixel to be covered by a random conformation. The toleranced balls cover the portion of the map D involving probabilities beyond a given threshold. Dashed lines represent the inner and outer balls of the toleranced balls. Note that higher the confidence / probability, the smaller the region between the inner and outer balls.

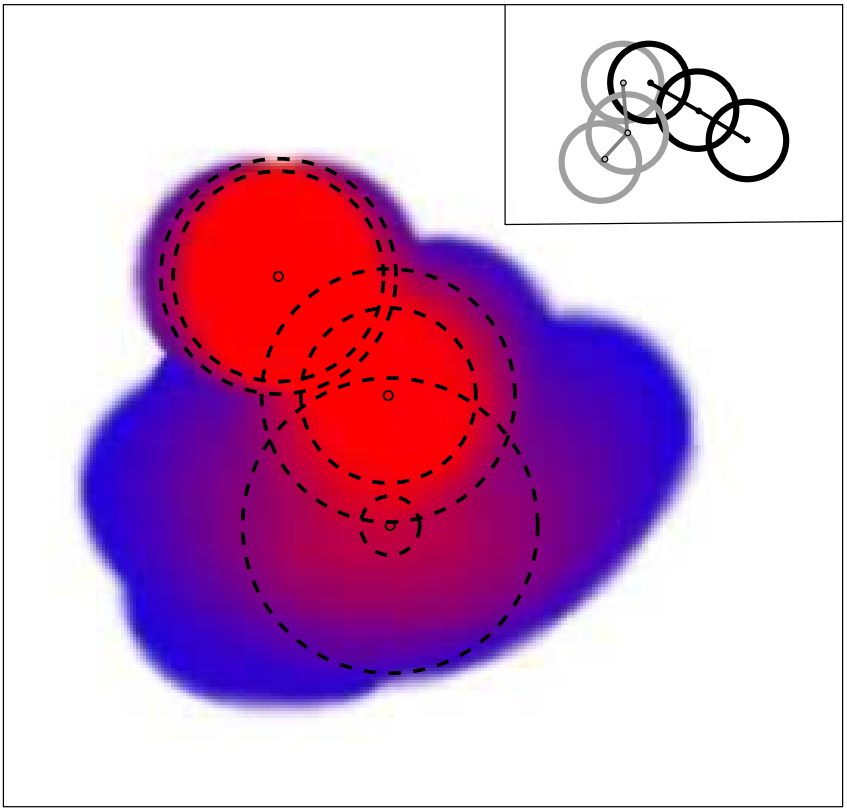

Figure 3 Toleranced tangent (TT) balls and conflict free balls. In dashed lines, toleranced balls $\overline{S_1}(0,0;1,5), \overline{S_2}(0,10;2,8), \overline{S_3}(4,-9;1,3)$. The three dotted circles represent $\overline{S_1}[3/4], \overline{S_2}[3/4], \overline{S_3}[3/4]$. The three circles centered at p are the scaled versions of ball $B(p,3/4)$; following remark 1, ball $B(p,3/4)$ is TT to $\overline{S_1}$ and $\overline{S_2}$, and conflict free with $\overline{S_3}$.

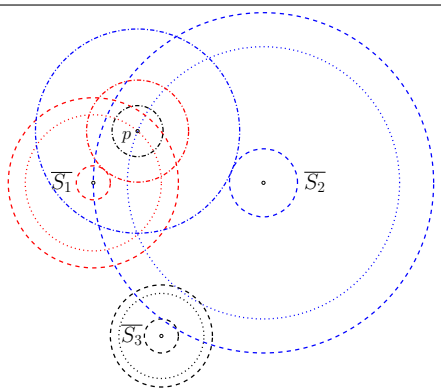

Figure 4 Two toleranced balls and their bisector which is a degree four algebraic curve –green curve. Dashed circles corresponding to the inner and outer balls. Dotted circles correspond to the solutions of a degree four equation : blue ones are toleranced tangent circles, red ones are algebraic artifacts.

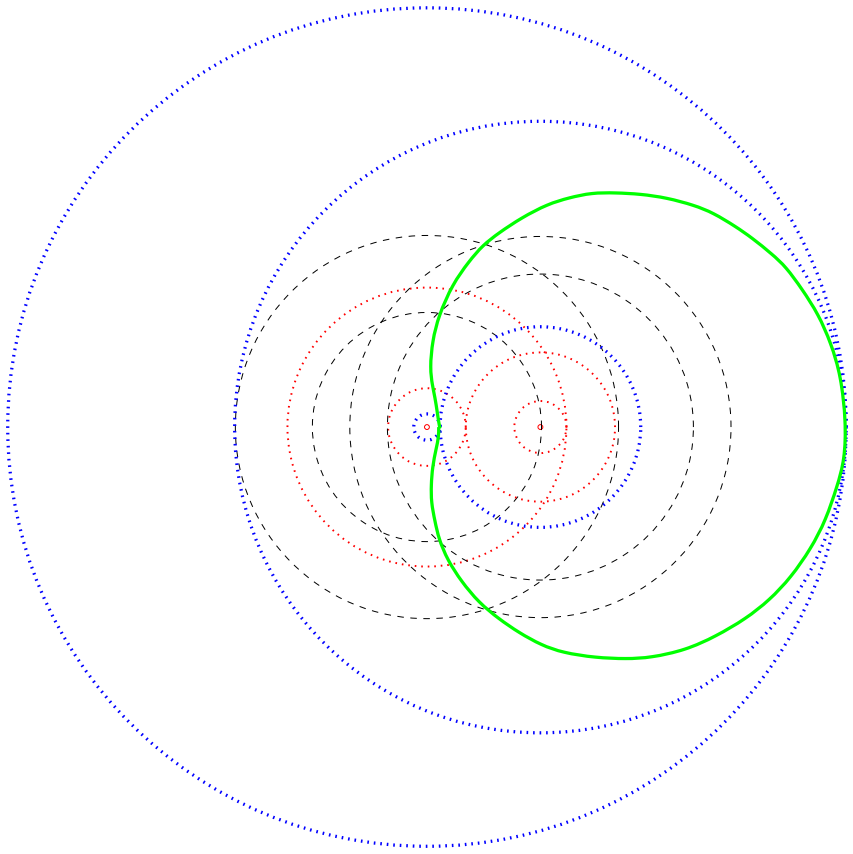

Figure 5 CW diagram and dual complex of 7 toleranced balls in 2D: $\overline{S_1} = (-5, -5; 3, 7)$, $\overline{S_2} = (5, 5; 3, 7)$, $\overline{S_3} = (-1, 0; 4, 5)$, $\overline{S_4} = (0, 0; 2, 5)$, $\overline{S_5} = (8, 7; 2, 3)$, $\overline{S_6} = (8, 5; 3, 4)$, $\overline{S_7} = (1, 10; 1, 2)$. $Vor(\overline{S_3})$ and $Vor(\overline{S_1}, \overline{S_2})$ are not connected. $Vor(\overline{S_2})$ is not simply connected. δ_1 and δ_2 are maximal and $\overline{S_1}, \overline{S_2}$ have unbounded Voronoi regions Conventions for the dual complex : 0-simplices: black dots; one-simplices: blue curves; two simplices: red dots. Note that $\overline{S_4}$ is represented by two vertices $\Delta_1(4)$ and $\Delta_2(4)$. $\Delta_1(2, 5, 6)$ and $\Delta_2(2, 5, 6)$ share the three same edges. $\Delta(2, 7)$ does not bound any triangle.

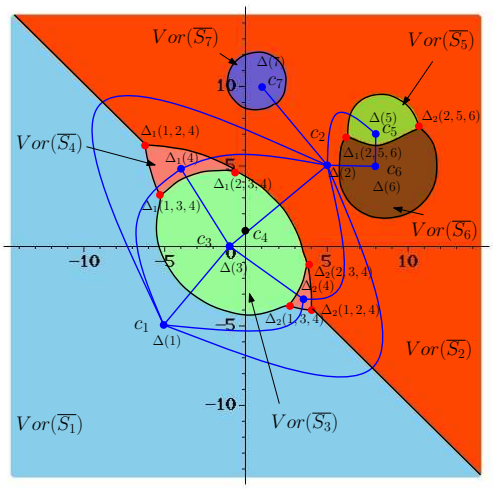

Figure 6 Dominant and dominated simplices illustrated with the CW VD of 3 toleranced balls (dashed lines): $\overline{S_1} = (5, 4; 1, 4)$ (black), $\overline{S_2} = (7, 7; 2, 3.5)$ (blue), $\overline{S_3} = (4, 5; 2, 3)$ (red). The max TT ball $\overline{M}_{\Delta(1,3)}$ is conflict free (witnessed by the blue dashed-dotted circle): $\Delta(1, 3)$ is dominant and $\Delta(3)$ is dominated. $\Delta(1, 2)$ is dominant and $\Delta(2)$ is dominated too.

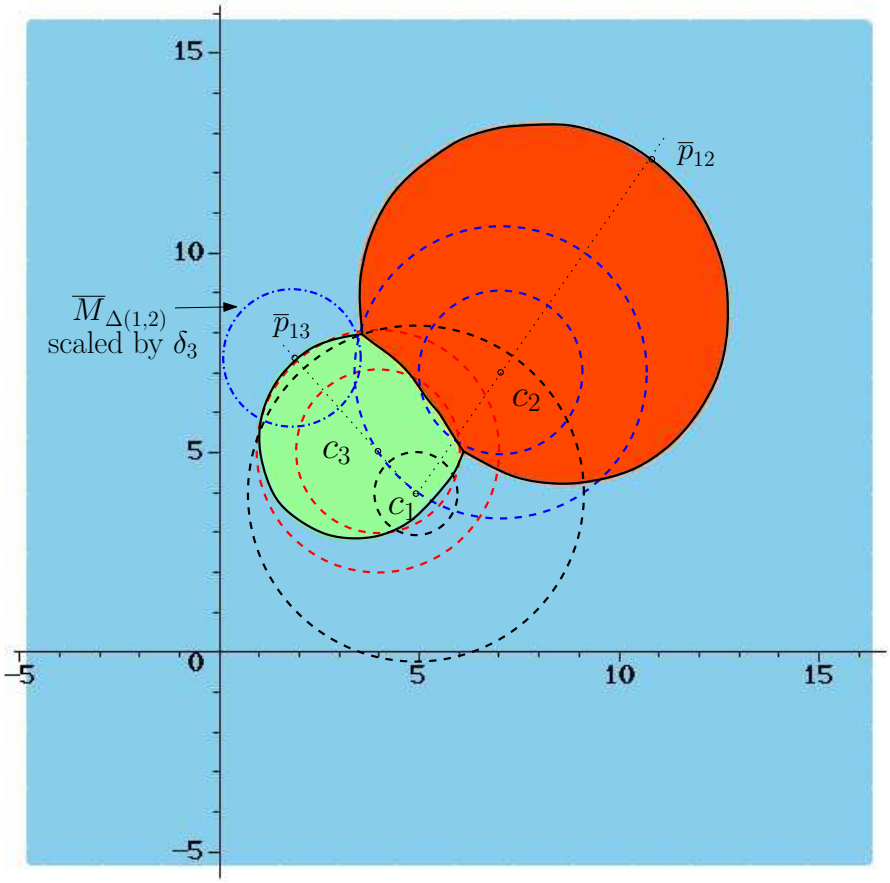

Figure 7 Restricted Voronoi regions for the CW VD of Fig. 5 for $\lambda = 1$. The 8 dual vertices and the 10 dual edges in the λ-complex are drawn in blue. $\Delta(5)$ and $\Delta(6)$ is interior and all other dual vertices are regular. There is no singular dual vertex. $\Delta(1,3)$ and $\Delta(2,7)$ are singular, $\Delta(2,3)$, $\Delta(2,5)$,$\Delta(2,6)$, $\Delta(5,6)$ are interior and all other dual edges are regular. The 4 dual triangles in the λ-complex are represented by red Voronoi vertices.

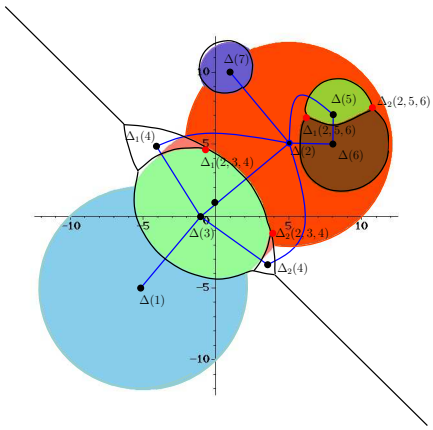

Figure 8 Half-spoke of the NPC : polyline connecting the points $(\#c.c., \lambda, r_\lambda)$; the λ values are those triggering a decrease of one unit of the number of connected components.

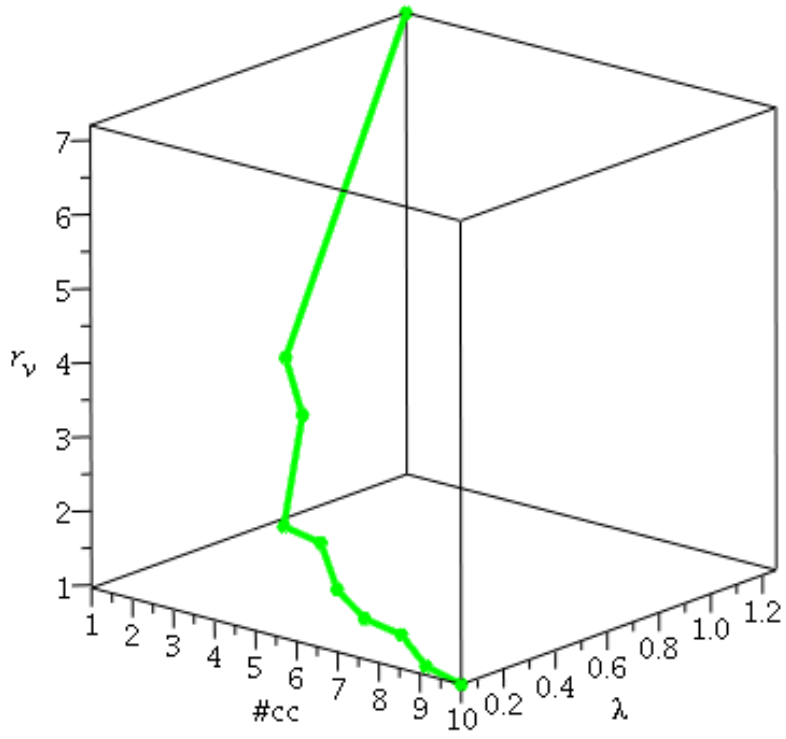

Figure 9 Half-spoke of the NPC : growing the balls in (a) so as to end up with a single connected component in (b). The volume of the right domain incurs a 7.2 fold ratio w.r.t. the volume of the isolated protein instances.

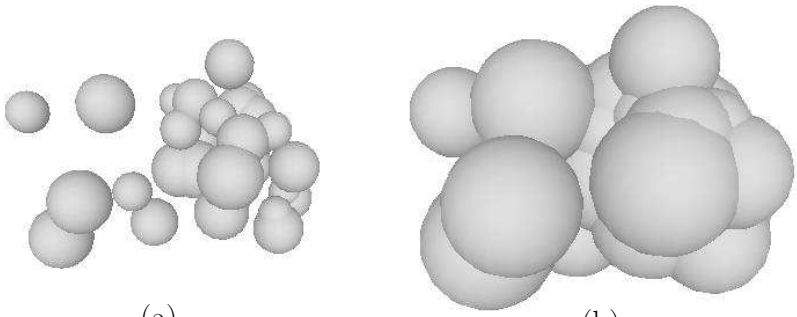

(a) (b)